Redox Biology 72 (2024) 103162

Contents lists available at ScienceDirect

Redox Biology

journal homepage: www.elsevier.com/locate/redox

Protein disulfide isomerase A1 regulates fenestration dynamics in primary mouse liver sinusoidal endothelial cells (LSECs)

Izabela Czyzynska-Cichon [a], Magdalena Giergiel [b], Grzegorz Kwiatkowski [a], Anna Kurpinska [a], Kamila Wojnar-Lason [a,e], Patrycja Kaczara [a], Marek Szymonski [b], Malgorzata Lekka [c], Ivars Kalvins [d], Bartlomiej Zapotoczny [b,c,*], Stefan Chlopicki [a,e,**]

[a] Jagiellonian University, Jagiellonian Centre for Experimental Therapeutics (JCET), Bobrzynskiego 14, 30-348, Krakow, Poland
[b] Jagiellonian University, Centre for Nanometer-Scale Science and Advanced Materials, NANOSAM, Faculty of Physics, Astronomy, and Applied Computer Science, Lojasiewicza 11, 30-348, Krakow, Poland
[c] Institute of Nuclear Physics Polish Academy of Sciences, Radzikowskiego 152, 31-342, Krakow, Poland
[d] Laboratory of Carbofunctional Compounds, Latvian Institute of Organic Synthesis, LV-1006, Riga, Latvia
[e] Jagiellonian University Medical College, Faculty of Medicine, Department of Pharmacology, Grzegorzecka 16, 31-531, Krakow, Poland

A B S T R A C T

Protein disulfide isomerases (PDIs) are involved in many intracellular and extracellular processes, including cell adhesion and cytoskeletal reorganisation, but their contribution to the regulation of fenestrations in liver sinusoidal endothelial cells (LSECs) remains unknown. Given that fenestrations are supported on a cytoskeleton scaffold, this study aimed to investigate whether endothelial PDIs regulate fenestration dynamics in primary mouse LSECs.

PDIA3 and PDIA1 were found to be the most abundant among PDI isoforms in LSECs. Taking advantage of atomic force microscopy, the effects of PDIA1 or PDIA3 inhibition on the fenestrations in LSECs were investigated using a classic PDIA1 inhibitor (bepristat) and novel aromatic *N*-sulfonamides of aziridine-2-carboxylic acid derivatives as PDIA1 (C-3389) or PDIA3 (C-3399) inhibitors. The effect of PDIA1 inhibition on liver perfusion was studied *in vivo* using dynamic contrast-enhanced magnetic resonance imaging. Additionally, PDIA1 inhibitors were examined *in vitro* in LSECs for effects on adhesion, cytoskeleton organisation, bioenergetics, and viability.

Inhibition of PDIA1 with bepristat or C-3389 significantly reduced the number of fenestrations in LSECs, while inhibition of PDIA3 with C-3399 had no effect. Moreover, the blocking of free thiols by the cell-penetrating *N*-ethylmaleimide, but not by the non-cell-penetrating 4-chloromercuribenzenesulfonate, resulted in LSEC defenestration. Inhibition of PDIA1 did not affect LSEC adhesion, viability, and bioenergetics, nor did it induce a clear-cut rearrangement of the cytoskeleton. However, PDIA1-dependent defenestration was reversed by cytochalasin B, a known fenestration stimulator, pointing to the preserved ability of LSECs to form new pores. Importantly, systemic inhibition of PDIA1 *in vivo* affected intra-parenchymal uptake of contrast agent in mice consistent with LSEC defenestration.

These results revealed the role of intracellular PDIA1 in the regulation of fenestration dynamics in LSECs, and in maintaining hepatic sinusoid homeostasis.

1. Introduction

The functioning of cells is highly dependent on the regulatory mechanisms responsible for the correct folding and conformational changes of proteins that lead to the activation or deactivation of biological pathways. Among this molecular machinery, the protein disulfide isomerase (PDI) family is considered to be one of the most abundant and critical biocontrollers. PDIs catalyze the formation, breakage and rearrangement of disulfide bonds, making them crucial to cysteine-based redox protein folding in the endoplasmic reticulum [1]. However, since the folding function of PDIs was first described nearly 60 years ago, knowledge of the various roles of PDIs in both physiological and pathological processes has expanded significantly and includes the regulation of angiogenesis and thrombus formation, as well as their involvement in the pathogenesis of cardiovascular disease and cancer [1,2].

Interestingly, several studies have underlined the PDIs' contribution to cytoskeleton rearrangement by regulating cell adhesion or directly affecting cytoskeletal organisation. This activity of PDIs is related to the reversible modifications of cysteines in redox-sensitive proteins, which affect their function [3–5]. The best-known example of this type of regulation refers to thiols in αIIbβ3 platelet receptors. The activity of PDIs supports platelet aggregation and thrombosis by reduction of disulfide bonds in αIIbβ3, resulting in conformational changes and

* Corresponding author. Institute of Nuclear Physics Polish Academy of Sciences, Radzikowskiego 152, 31-342, Krakow, Poland
** Corresponding author. Jagiellonian University, Jagiellonian Centre for Experimental Therapeutics (JCET), Bobrzynskiego 14, 30-348, Krakow, Poland
E-mail addresses: bartlomiej.zapotoczny@ifj.edu.pl (B. Zapotoczny), stefan.chlopicki@jcet.eu (S. Chlopicki).

https://doi.org/10.1016/j.redox.2024.103162
Received 15 February 2024; Received in revised form 6 April 2024; Accepted 15 April 2024
Available online 16 April 2024

integrin activation [4]. A similar type of regulation catalyzed by extracellular PDIs was also reported for other integrins, including αVβ3 and α11β1 receptors [6,7]. On the other hand, in response to outside-in integrin activation, intracellular PDIs were shown to form a complex directly with β-actin and modify its structure through Cys 374 oxidation, repositioning the cytoskeleton during megakaryocyte adhesion [5]. Moreover, total silencing of the intracellular PDIA1 isoform in vascular smooth muscle cells (VSMC) contributed to cytoskeletal disruption through altered NADPH-derived reactive oxygen species (ROS) generation and downregulation of the RhoA/Rac1 pathway [8], underscoring a possible involvement of intracellular PDIs in the regulation of cytoskeletal rearrangement.

The organisation of the cytoskeleton is of particular importance for liver sinusoidal endothelial cells (LSECs) to maintain their unique fenestrated structure. Fenestrations represent a special type of transcellular nanopore (50–350 nm in diameter) organized in sieve plates, which are fundamental to the LSECs' function: the bidirectional transport of macromolecules, especially lipoproteins, between the blood and the liver parenchyma. Fenestrated endothelium opens access to the underlying space of Disse, which additionally expands hepatic microvascular perfusion volume [9]. The size of the perfusion area regulated by LSEC porosity determines blood flow velocity and maintains homeostasis of hepatic sinusoids responsible for proper liver function [10,11]. The presence of fenestrations is a characteristic feature of healthy LSECs, while their loss is associated with ageing and various liver diseases, such as nonalcoholic fatty liver disease, nonalcoholic steatohepatitis, liver fibrosis, cirrhosis, and hepatitis C [12–17]. Moreover, LSEC defenestration was correlated with reduced hepatic uptake of chylomicron remnants resulting in elevated levels of circulating lipids and hyperlipidemia [18]. Therefore, maintaining fenestrated endothelial barrier as a part of the communication and filtration system between the liver and circulation is essential for proper liver physiology and homeostasis.

The structure of fenestrations is supported on the actin/spectrin scaffold, which allows active regulation of their size and number [19]. However, the mechanisms behind the dynamics of fenestrations are still not fully understood. A recent study has demonstrated that the diamide or iodoacetic acid caused destabilisation of the cytoskeleton and significant changes in the number of fenestrations, that were attributed to the oxidation of thiol groups of spectrin [19]. These results suggest that the thiol-dependent mechanisms of cytoskeleton rearrangement might play an important role in the regulation of fenestration dynamics in LSECs. However, it is not known whether PDIs, the major oxidoreductase enzymes responsible for disulfide exchange reactions that modulate the function of multiple proteins, including the cytoskeleton [5,20], are involved in the redox-dependent regulation of fenestrations.

Therefore, the present work aimed to investigate a possible contribution of the most abundant endothelial PDI isoforms – PDIA1 and PDIA3 [21] – in regulating fenestration dynamics in primary mouse LSECs. Comprehensive studies of the porosity, function and organisation of the LSEC cytoskeleton in response to the inhibition of PDIA1 and PDIA3 revealed that intracellular PDIA1, but not PDIA3, plays an important role in regulating fenestrae. Furthermore, *in vivo* experiments confirmed that PDIA1-dependent defenestration impairs the sinusoidal perfusion capacity and thus disturbs hepatic sinusoid homeostasis.

2. Experimental protocols

2.1. Reagents

2.1.1. PDI inhibitors and thiol agents

Bepristat 2a hydrochloride (bepristat) used as a reference inhibitor against PDIA1, was obtained from Sigma-Aldrich (Saint Louis, MO, USA). Additionally, the recently developed aromatic *N*-sulfonamides of aziridine-2-carboxylic acid derivatives, C-3389 and C-3399, were used as pharmacological tools for PDIA1 and PDIA3 inhibition [22]. Previously performed an insulin turbidimetric assay revealed that C-3389 was a potent and selective PDIA1 inhibitor, while C-3399 was a PDIA3 inhibitor with a much weaker inhibitory effects on PDIA1 as compared with C-3389 (Table S1) [22].

N-ethylmaleimide (NEM) (Sigma-Aldrich, Saint Louis, MO, USA) and 4-Chloromercuribenzenesulfonate (pCMBS) (Toronto Research Chemicals, Toronto, Canada) were used as reference tools to confirm the role of thiols and to distinguish whether intracellular or extracellular sulfhydryl groups are involved. pCMBS is a membrane-impermeant reagent acting on sulfhydryl groups of the membrane surface while NEM is a cell-penetrating thiol-alkylating agent.

2.1.2. Other reagents

Cytochalasin B (CytB), ML171 and Poloxamer 407 were obtained from Sigma-Aldrich (Saint Louis, MO, USA). Y27632 dihydrochloride (Y27632) and PF573228 were purchased from Tocris Bioscience (Bristol, UK). Primary antibodies *anti*-pMLC (Ser19) (3671 S) and *anti*-ppMLC (Thr18/Ser19) (95777 S) were from Cell Signalling Technology (Danvers, MA, USA), while *anti*-P4HB (PDIA1; ab137110) and *anti*-ERp57 (PDIA3; ab13506) were purchased from Abcam (Cambridge, UK). The secondary antibodies goat anti-rabbit Alexa Fluor 647-conjugated, goat anti-rabbit Cy3-conjugated and goat anti-mouse Cy3-conjugated were produced by Jackson Immuno Research Labs (Baltimore Pike, PA, USA). The fluorescent indicators: CM-H_2DCFDA, Alexa Fluor 488 Phalloidin, DAPI and Hoechst came from Invitrogen (Waltham, MA, USA). Dimethyl sulfoxide (DMSO) (Sigma-Aldrich, Saint Louis, MO, USA) and POLIkol 300 (Polikol 300) (PCC Exol, Poland) were used as solvents for compounds insoluble in water.

2.2. LSEC isolation

The primary LSECs were isolated from C57BL/6 mice (Medical University of Bialystok, Poland) according to the protocol presented by Smedsrød and Pertoft (1985) [23] with further modifications [24]. Briefly, blood was washed out from the livers through the portal vein with perfusion buffer (37°C) and connective tissue was digested with buffered collagenase (Liberase TM, Roche, Switzerland). Next, the cell suspension was differentiated by a series of low-speed centrifugations followed by gradient density sedimentation in 25–50 % Percoll (Cytiva) to obtain the non-parenchymal cell fraction. In the final step, LSECs were purified by immunoseparation using LSEC-specific CD146 magnetic MicroBeads (MACS, Miltenyi Biotec, Germany). Prior to the experiments, freshly isolated LSECs were incubated overnight in EGM-2 medium (Lonza, Switzerland) supplemented with 2 % FBS under 37°C and 5 % CO_2 conditions. All experimental procedures, except adhesion studies, were performed within 12–18 h after cell seeding, as this approach was shown to preserve fenestrations in primary LSECs [19,25].

2.3. Identification and quantification of PDI and integrin isoforms in primary mouse LSECs using a proteomic approach

LSEC lysates were prepared according to the protocol by Sitek et al. (2012) [26] Briefly, cell pellets were lysed in lysis buffer containing 7 M urea (BioShop, Canada), 2 M thiourea (BioShop, Canada), and 30 mM Tris-HCl (pH 8.0) (BioShop, Canada), sonicated on ice and centrifuged (16,000 g, 15 min, 4 °C). The total protein content in each sample (supernatant) was measured with Bradford assay-Quick Start Bradford 1x Dye Reagent (Bio-Rad, CA, USA). Proteins were reduced, alkylated and digested. The resulting peptides were analysed using LC-MS/MS and acquired data were processed as described previously [27–29]. The repertoires of PDI and integrin isoforms were semiquantified using the exponentially modified protein abundance index (emPAI) normalised to the overall protein composition (emPAI %) [30,31].

2.4. Quantification of fenestrations, evaluation of cell morphology, and determination of Young's (elastic) modulus by atomic force microscopy (AFM)

The AFM measurements were conducted using Nanowizard 4 (Bruker-JPK Instruments, Germany), and part of the morphological analysis of bepristat-treated cells was performed based on data recorded using Nanowizard 3 (JPK Instruments, Germany). Determination of fenestration number was performed according to previously described protocols [19,32]. Briefly, freshly isolated LSECs were cultured for 8–20 h and fixed using 1 % (v/v) glutaraldehyde for 2 min prior to measurements. Detailed images of cell morphology were collected in Quantitative Imaging (QI) mode with a point-to-point resolution of <90 nm. SCM-PIC-V2 (Bruker, Germany) cantilevers were used with the loading force ranging from 0.2 to 0.3 nN adjusted to the scanning conditions. Obtained images of topography and stiffness were used for further analysis.

The number of fenestrae per area (defined as fenestrae frequency, fen./μm^2) in each image was quantified based on the automatic and precise approach using a neural network algorithm described previously [33]. Cell height was calculated using cross-sections of the topography images of fixed cells. The maximal observed values were compared between groups. Young's (elastic) modulus values were determined in live LSECs within 8–24 h. Two types of measurements were performed. The first method, based on force-distance curves, was applied. Maps of 6 × 6 μm^2 were collected with 6 × 6 force-distance curves. MLCT-BIO-DC (Bruker) were selected for the measurements (k = 0.1 N/m, loading force of 1.0 nN, acquisition speed 8 μm/s, z length 5 μm). 15–20 cells per group per animal were measured and analysed. Young's modulus was calculated based on the Hertz-Sneddon model, assuming that a cone can approximate the tip apex. Commercial software JPKSPM Data Processing was used. The QI mode provided elasticity maps of whole cells (Fig. S2 A-C). A loading force of 0.3 nN was applied to minimize the effect of the glass substrate and visualise the cortical cytoskeleton [25]. Force curves collected in each pixel-point were analysed, and reconstructed images of topography and elastic modulus were presented.

2.5. Assessment of microvascular liver perfusion using dynamic contrast-enhanced magnetic resonance imaging (DCE-MRI)

MRI measurements were performed using a commercial small-animal MRI 9.4 T scanner (Bruker BioSpec, Ettlingen, Germany) equipped with a 36 mm T/R RF coil (Department of Magnetic Resonance Tomography at the Institute of Nuclear Physics of the Polish Academy of Sciences in Krakow). The experimental procedure was adapted from Byk et al. (2016) [34]. For imaging, animals were sedated using inhalation anaesthesia with isoflurane in a mixture of oxygen and air (1:2 ratio), 3 % isoflurane was used to induce anaesthesia and 1.5 %–1.75 % isoflurane was used to maintain anaesthesia inside the scanner. Throughout the measurement, mice were housed in a dedicated measurement bed equipped with a heating system. Body temperature, heart function (ECG) and respiration were continuously monitored. The heating system and the intensity of anaesthesia were adjusted accordingly to achieve stable body temperature (36–37 °C) and stable respiration (50–70 breaths per minute). Bepristat (10 or 30 mg/kg b. w. [35]) was injected intravenously 20 min before DCE-MRI measurements. Poloxamer 407 (1 g/kg b. w.), a surfactant that induces extensive defenestration of LSECs both *in vivo* and *in vitro*, was used as a positive control and was administered *i. p.* 24 h before the experiment, according to a previously published protocol [36].

A hepatocyte-specific contrast agent, administered via a tail vein catheter at a dose of 10 μL/1 g b. w. 0.0025 mmol (Primovist, Bayer Schering Pharma AG, Germany), was used to assess liver perfusion. DCE-MRI was performed using a retrospectively gated IntraGateFLASH sequence (ParaVision 6.0.1, Bruker, Ettlingen, Germany) with the following parameters: TE 2.23 ms, TR 6.60 ms, number of repetitions per image 42, number of dynamic images = 252, flip angle 18°, FOV 30 × 30 mm^2, image size 128 × 128, slice thickness = 1 mm. The imaging slice was placed along the transverse axis of the body and rotated at an angle of 15–30° to avoid the stomach and maximize the area of the liver in the field of view. The navigator layer was placed in the short axis of the heart with the layer thickness = 8 mm and RF flip angle = 45°. The total DCE-MRI measurement time was 42 min.

For data analysis, the reconstructed MR images were loaded into the Matlab environment (Mathworks, USA). To obtain the amplitude of the MRI signals in the liver microcirculation and respective changes after contrast administration, an image mask was created that contained only the liver parenchyma, without the large vessels, muscle, fat, and gall bladder. For this purpose, the outer contour of the liver was outlined manually. Then, the signal level was tresh-holded so that no large blood vessels were visible. The obtained mask was applied to all the dynamic images resulting in the mean MRI signal in the liver parenchyma for each time frame. The obtained signal enhancement versus time curves were analysed quantitatively. The total area under the curve and maximum enhancement were determined.

Procedures involving animals were performed in accordance with the Guide for the Care and Use of Laboratory Animals Directive 2010/63/EU of the European Parliament) and approved by the 2nd Local Institutional Animal Care and Use Committee in Krakow (agreement no. 183/2023).

2.6. Immunocytochemistry of primary mouse LSECs

To evaluate the PDIA1 and PDIA3 distribution in primary mouse LSECs as well as the degree of myosin phosphorylation and quality of actin filaments in response to PDIA1 inhibition, the immunocytochemistry technique was applied. First, LSECs were treated with PDI and actomyosin inhibitors or their combinations in an EGM-2 medium for 2 h at 37°C. Then, cells were washed with warm DPBS (Gibco) with calcium and magnesium, fixed with 4 % (w/v) paraformaldehyde (PFA) and permeabilized with either 0.1 % or 0.5 % (v/v) Triton X-100 solution for PDI and actin or *p*-MLC and pp-MLC staining, respectively. Before primary antibody incubation, nonspecific binding was blocked with 1 % (w/v) BSA solution in PBS (for pp-/p-MLC) or 5 % (v/v) normal goat serum (for PDIs) for 1 h at room temperature (RT). The primary antibodies *anti*-pMLC (Ser19) 1:100, *anti*-ppMLC (Thr18/Ser19) 1:50, *anti*-P4HB (PDIA1) 1:100 and *anti*-ERp57 (PDIA3) 1:100 were applied overnight at 4°C followed by 1 h incubation with goat anti-rabbit Alexa Fluor 647 (1:300), goat anti-rabbit Cy3 (1:300) or goat anti-mouse Cy3-conjugated secondary antibody (1:300) at RT. Actin filaments were stained independently with Alexa Fluor™ 488 Phalloidin (5:1000) for 30 min at RT. DAPI (1:2000) was used for nuclei counterstaining. The degree of myosin phosphorylation was assessed using a CQ1 imaging cytometer and Columbus v.2.4.2 software (PerkinElmer, Waltham, MA, USA). Pictures for qualitative analysis of PDIA1, PDIA3, actin, and myosin filaments were taken with either an Axio Imager. A2 fluorescent microscope (Carl Zeiss) or a Leica TCS SP8 WLL confocal microscope. For data presentation, images were post-processed with ImageJ 1.53q software using the Gaussian Blur filter with a value of 1.0 and correction of the minimum and maximum values of individual channels.

2.7. Western blotting analysis of spectrin βII expression in isolated mouse LSECs

LSEC samples containing 5 μg of total protein were loaded into a 7.5 % SDS-PAGE gel, followed by the protocol described in detail previously [19]. β-actin was used as a loading control.

2.8. Assessment of the cytotoxicity of the compounds

The impact of the studied compounds on LSEC viability was determined using a commercially available colorimetric assay: CellTiter 96®

AQueous Non-Radioactive Cell Proliferation Assay (MTS) (Promega, WI, USA), according to the manufacturer's instructions. Primary mouse LSECs were pre-incubated in the EBM-2 medium (Lonza, Switzerland) with the compounds for 2 h, followed by 1 h incubation in the presence of MTS reagents under 37°C and 5 % CO_2 conditions. After that time, the absorbance of the reduced MTS reagent was measured at 490 nm.

2.9. LSEC adhesion assay

To assess the effect of PDI inhibition on cell adhesion, freshly isolated LSECs were pre-incubated in suspension in EBM-2 medium containing the inhibitors for 30 min at RT. LSECs were then seeded at a density of 1 $\times$ 10^5 cells/well on differently coated surfaces: collagen I (10 μg/cm^2), fibronectin (1 μg/cm^2) and uncoated to verify the different adhesion pathways. For the next 2 h, the seeded LSECs remained exposed to the compounds at 37°C and 5 % CO_2. After that time, LSECs were washed with warm DPBS with calcium and magnesium to remove unattached cells and fixed with 4 % (w/v) PFA. To quantify the number of cells adhered to the surface, LSEC nuclei were stained with Hoechst (1:2000) and visualized using a CQ1 image cytometer (Yokogawa, Japan). The number of LSECs was calculated using Columbus v.2.4.2 software (PerkinElmer, Waltham, MA, USA).

2.10. Assessment of LSECs bioenergetics

The effects of PDIA1 inhibition on the metabolism of isolated LSECs were evaluated using a Seahorse XFe 96 Analyzer (Agilent Technologies, USA), which enables simultaneous real-time measurements of oxygen consumption (OCR) and extracellular acidification (ECAR), which reflect mitochondrial respiration and glycolysis, respectively. Briefly, LSECs were preincubated for 2 h with 10 μM bepristat or C-3389, followed by Seahorse Mitochondrial Stress Test (MST) and Glycolysis Stress Test (GST) as previously described [24].

2.11. Measurements of ATP production

The effects of 2 h of PDIA1 inhibition on ATP production in primary mouse LSECs were studied with the ATPlite 1 step Luminescence Assay System (PerkinElmer, Waltham, MA, USA) according to the manufacturer's instructions.

2.12. Detection of reactive oxygen species

The intracellular ROS generation was detected using CM-H_2DCFDA fluorescent probe. Prior to the assay LSECs were serum starved overnight in EBM-2 medium. Next, cells were treated with bepristat (10 μM), ML171 (5 μM), and apocynin (100 μM) for 2 h at 37°C, followed by loading with DCF probe (10 μM) in HBSS for 30 min at 37°C. ROS generation was assessed by measurements of the fluorescence intensity obtained with the CQ1 imaging cytometer (Yokogawa, Japan). Image analysis was performed using Columbus v.2.4.2 software (PerkinElmer, Waltham, MA, USA).

2.13. Statistical analysis

Results are presented as mean values with standard deviation unless otherwise stated. Shapiro-Wilk and Levene's tests were used to examine data distribution normality and variance homogeneity. Based on the variable properties and the nature of the comparison, Student's t-test, two-way ANOVA followed by Tukey post-hoc test or the non-parametric Kruskal-Wallis were used to assess statistical significance between experimental groups. P-values less than 0.05 were considered significant. Statistical verification was performed using Statistica 13.3.

3. Results

3.1. The proteomic-detected repertoire of PDI isoforms and different distributions of PDIA1 and PDIA3 in the primary murine LSECs

Using a proteomic approach, the repertoire of 10 PDI isoforms was identified in LSEC lysates, among which PDIA3 and PDIA1 were found to be the most abundant, reaching 0.96 and 0.65 emPAI %, respectively (Fig. 1A). Interestingly, immunostaining revealed a different cellular distribution of these two major isoforms of PDI in primary mouse LSECs. While PDIA3 occurrence was limited to the perinuclear zone, PDIA1 distribution pattern extended from the perinuclear area to the cell periphery (Fig. 1B and C), which may indicate distinct functions of these two isoforms in LSECs.

3.2. Inhibition of PDIA1 reduced the number of fenestrations in the primary mouse LSECs

To distinguish whether PDIA1 or PDIA3 might be involved in regulating LSEC porosity, the novel aromatic *N*-sulfonamide of aziridine-2-carboxylic acid derivatives with an increased selectivity towards PDIA1 (C-3389) and with relative selectivity towards PDIA3 (C-3399) were used (see **Experimental Protocols** section). Additionally, to confirm the involvement of PDIA1, a selective reference inhibitor, bepristat, was used to block PDIA1 activity.

The AFM measurements in fixed LSECs revealed that inhibition of PDIA1 with both C-3389 and bepristat resulted in a significant reduction in the number of fenestrations after 2 h of drug treatment compared to the untreated cells (Fig. 2A and B, E-G). The effect of bepristat was dose-dependent and slightly less pronounced than C-3389. This difference in potency was further confirmed by real-time measurements in living cells, demonstrating the acute effects of PDIA1 inhibitors on LSEC fenestrations. As shown in Figs. S1A and C and Movie S1, administration of bepristat (10 μM) caused a gradual decrease in the number of fenestrae in living LSECs over the course of approximately 1 h, while effects of C-3389 (10 μM) were already clearly visible after ca. 30 min (Figs. S1B and D, Movie S2). Stronger and faster effects of the novel C-3389 compound in closing fenestrations were consistent with the higher potency of C-3389 to inhibit PDIA1 in the isolated enzyme assay (Table S1) [22]. Interestingly, neither bepristat nor C-3389 completely blocked the formation of fenestrations, as new pores were still observed, suggesting impaired dynamics of fenestrae formation and closure.

Supplementary video can be found at https://doi.org/10.1016/j.redox.2024.103162

In contrast to the clear-cut effects of PDIA1 inhibition, the relative blockage of PDIA3 by C-3399 did not alter LSEC porosity (Fig. 2H and I), pointing to a distinct role of PDIA3 and PDIA1 in LSEC functioning and inability to compensate for each other in the regulation of fenestration dynamics.

3.3. Inhibition of PDIA1 alters the in vivo dynamics of contrast agent uptake in the liver parenchyma

Given that fenestrated endothelium constitutes the liver ultrafiltration system [18,36–38], it was investigated whether inhibition of PDIA1 has physiological consequences resulting in changes in sinusoidal perfusion capacity. Alternations in the dynamics of hepatocyte-specific contrast agent uptake through the liver microcirculation were examined using DCE-MRI. A single administration of bepristat, at a dose of 30 mg/kg b. w., significantly limited the uptake of the contrast agent into the liver and the effect was comparable to the effect of the poloxamer 407 pre-treatment (Fig. 3). Lower dose of bepristat (10 mg/kg b. w.) tended to decrease maximum contrast enhancement although it was statistically insignificant ($P = 0.0679$). These results indicate that PDIA1 inhibition impaired sinusoidal perfusion, which largely depends on LSEC fenestrations and function [18,34,36].

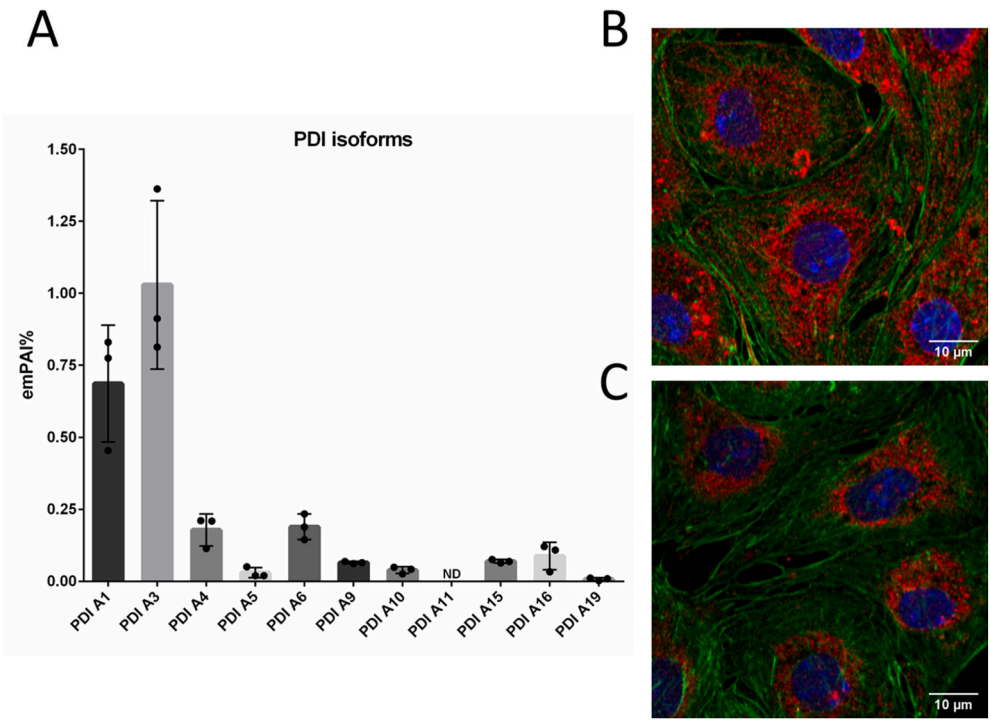

Fig. 1. Repertoire and localisation of PDI isoforms in primary mouse LSECs. Levels of PDI enzymes detected with proteomic analysis (A) and cellular distribution of PDIA1 (B) and PDIA3 (C) visualized by confocal microscopy. ND – not detected. Red fluorescence – PDIA1 or PDIA3; green fluorescence – actin. (For interpretation of the references to color in this figure legend, the reader is referred to the Web version of this article.)

3.4. Modulation of intracellular rather than extracellular thiols affected fenestration dynamics in primary mouse LSECs

Given that PDIs might be involved in integrin-dependent outside-in signalling in response to the adhesion of cells to the extracellular matrix [5], the proteomic-detected repertoire of integrins in LSECs was investigated, as well as their possible involvement in the regulation of LSEC adhesion and fenestration dynamics. The LSEC proteome displayed seven integrin isoforms, of which the β-1 and α-1 integrins were the most highly expressed (Fig. 4A). However, despite a wide range of proteomic-detected integrins, inhibition of PDIA1 by either bepristat or C-3389 did not affect LSECs' ability to adhere to collagen I, fibronectin or uncoated surface as compared to the untreated cells (Fig. 4B–D) suggesting integrin-independent mechanisms of adhesion and fenestrate regulation in isolated murine LSECs. PF573228 (1 μM), the focal adhesion kinase (FAK) inhibitor, used as a positive control, also did not diminish LSEC adhesion to collagen I, fibronectin or uncoated surface, which may indicate extremely strong attachment of LSECs in this experimental setup and the involvement of other integrin-dependent mechanisms in LSEC surface adhesion.

To further confirm that intracellular, but not extracellular, mechanisms are primarily involved in regulating fenestration dynamics, LSECs were treated either with pCMBS, acting on the sulfhydryl groups of the membrane surface, or NEM, a cell-penetrating thiol-alkylating agent. The number of fenestrations was visibly decreased in the presence of low micromolar concentrations of NEM in a dose-dependent manner (Fig. 5A and B), while LSECs incubated with the high concentration of pCMBS (100 μM) had fully preserved porosity as compared to untreated cells (Fig. 5C and D). Moreover, the elasticity of the LSECs treated with NEM (3 μM) was significantly impaired (increased Young's modulus in comparison to the control), indicating cell stiffening (Figs. S2C and D).

3.5. PDIA1 inhibition did not affect LSEC viability and bioenergetics

To exclude a possible involvement of toxic effects on LSEC function in PDIA1-mediated regulation of fenestration dynamics, LSEC viability and bioenergetics in response to PDIA1 inhibition were assessed. Neither bepristat nor C-3389 given at a concentration that induced substantial defenestration (see Fig. 2) decreased the LSEC viability or altered basal ATP production (Fig. 6A–C). Mitochondrial respiration and glycolysis were also preserved in LSECs treated with bepristat (10 μM) for 2 h, confirming a lack of effect of PDIA1 inhibition on bioenergy metabolism. However, administration of C-3389 (10 μM) for 2 h moderately decreased basal respiration (by reducing OCR related to ATP production), maximal respiration (under the condition of energy stress induced by FCCP) and spare respiratory capacity. Simultaneously, a transient increase in basal glycolysis in LSECs, at the expense of glycolytic reserve, was observed during the first hour after the administration of C-3389 (10 μM) (Fig. 6D and E).

3.6. Lack of effects of NADPH oxidase inhibition on LSEC fenestrations

Since PDIA1 has been shown to be essential for vascular smooth muscle cell migration by regulating NADPH oxidase 1 (NOX1) activity [8], the effect of NOX inhibition on LSEC porosity was investigated. As shown in Figs. S3A and C and Movie S3 the inhibition of NOX with ML171 (5 μM) did not alter the number of fenestrae as compared to the control in both fixed and living cells. Moreover, DCF-based ROS detection revealed a decrease in ROS generation in LSECs in response to ML171, but not in response to bepristat (Fig. S3B), indicating that PDIA1 regulates LSEC porosity by a NOX-independent pathway. A similar trend was observed for another NOX inhibitor – apocynin, however, the effect was not significant.

Supplementary video can be found at https://doi.org/10.1016/j.redox.2024.103162

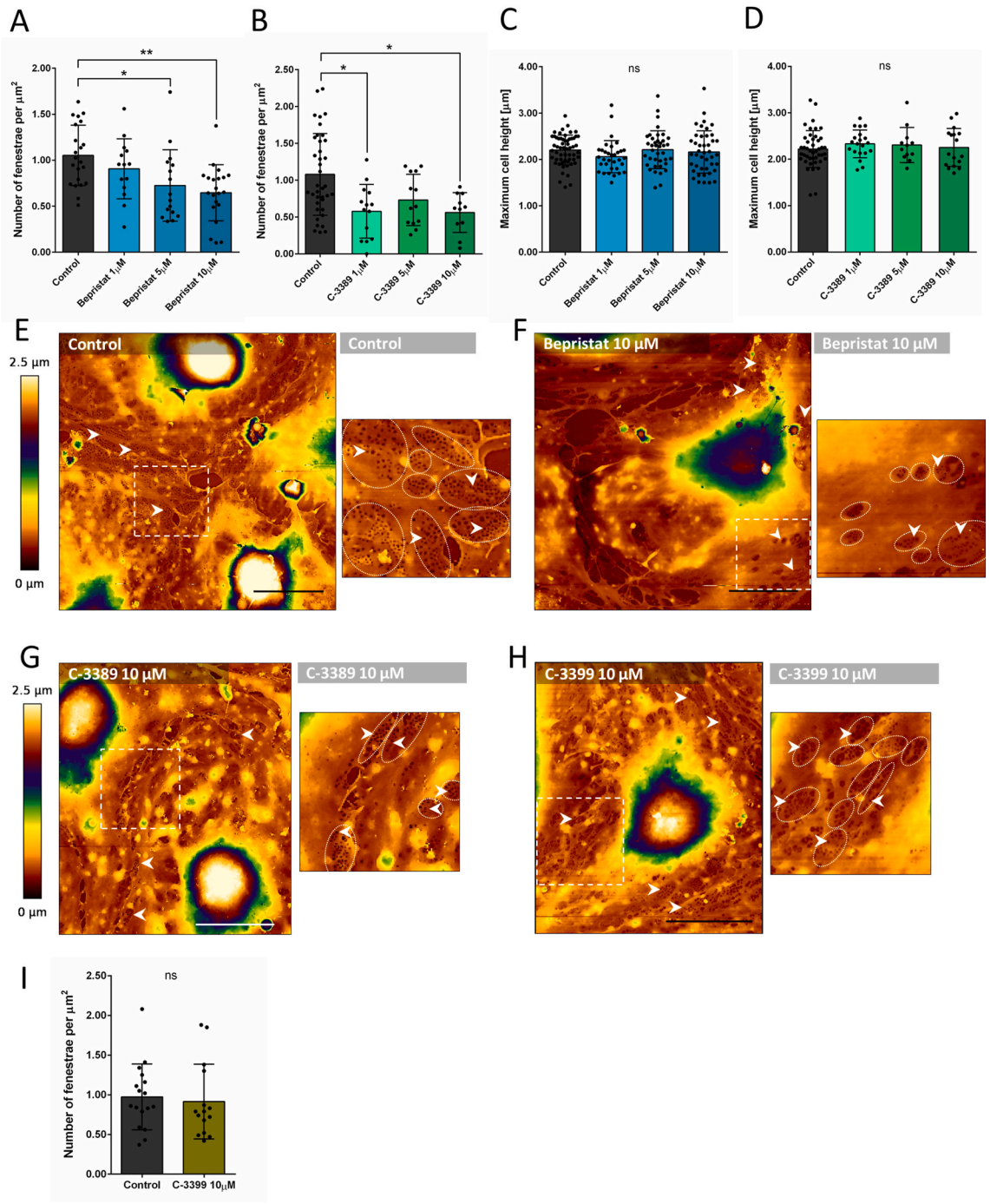

Fig. 2. The effects of PDIA1 and PDIA3 inhibition on fenestrations in primary mouse LSECs. The number of fenestrae (A, B), maximum cell height (C, D), and representative images of morphological changes in primary LSECs (E, F, G) in response to increasing concentrations of the PDIA1 inhibitors, bepristat and C-3389, assessed *in vitro* by AFM. The LSEC porosity after inhibition of PDIA3 with 10 µM C-3399 (H, I). The scale bars refers to the sample height, where range between 0 and 2.5 µm corresponds to the surface (glass coverslip) and to the highest point of the cell (nucleus), respectively. Fenestrae (white arrows) are visible as dark spots organized in sieve plates at the height corresponding to the surface.
Scale bars – 10 µm. The graphs show the mean values ± SD of individual AFM images (n = 11–38) corresponding to 3–4 biological replications. *P ≤ 0.05, **P ≤ 0.01 significantly different vs control group, ns – not statistically significant.

3.7. The effect of PDIA1 inhibition on LSEC fenestrations was not associated with a significant cytoskeleton reorganisation and was completely overcome by cytochalasin B-induced actin depolymerisation

To verify whether PDIA1-dependent defenestration was linked to reorganisation of the cytoskeleton, spectrin β II expression, the degree of the myosin (di)phosphorylation and actin polymerisation were examined. Additionally, the impact of PDIA1 inhibition on actomyosin in LSECs was compared with the effects of the reference cytoskeletal agents: Y27632 (the ROCK inhibitor limiting myosin phosphorylation) and cytochalasin B (the gold standard for stimulating LSEC porosity), as well as the cell-penetrating thiol exchange inhibitor, NEM. In contrast to the previously described effects of diamide [19], bepristat (10 µM) did not alter spectrin β II expression in primary mouse LSECs compared to the untreated cells (Fig. 7A) indicating a distinct mechanism of action. The degree of myosin phosphorylation also remained unchanged after

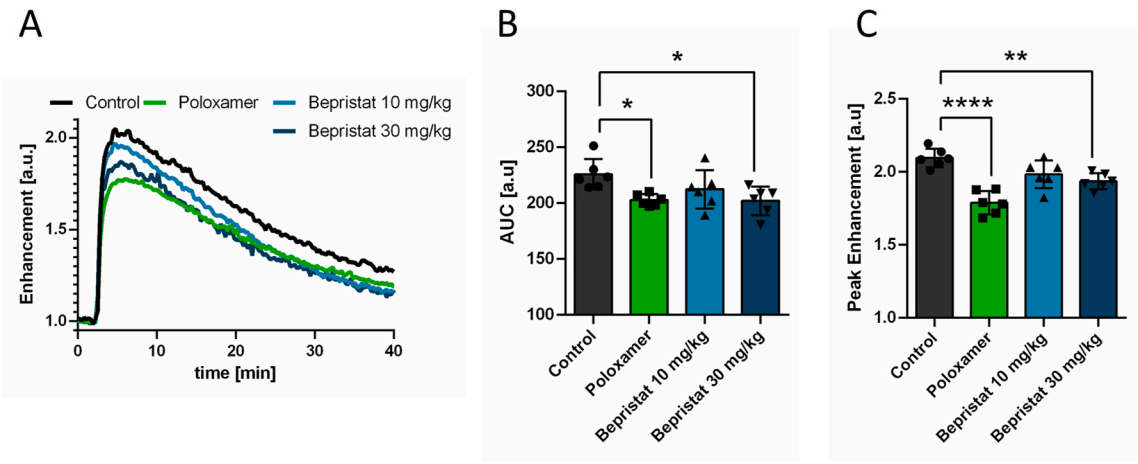

Fig. 3. The effect of PDIA1 inhibition on the *in vivo* dynamics of contrast agent uptake in the liver parenchyma. The readout of magnetic resonance imaging with dynamic contrast enhancement (DCE-MRI) was based on contrast enhancement time-dependent curves (A), calculated area-under-the-curve (AUC) (B) and maximal contrast enhancement (C). Results were obtained from the whole livers in control animals, pre-treated with poloxamer 407 (1 g/kg b. w.) and after single administration of bepristat (10 or 30 mg/kg b. w.) (n = 6).
Data are presented as mean values ± SD. *P ≤ 0.05, **P ≤ 0.01, ***P ≤ 0.001 significantly different vs control group.

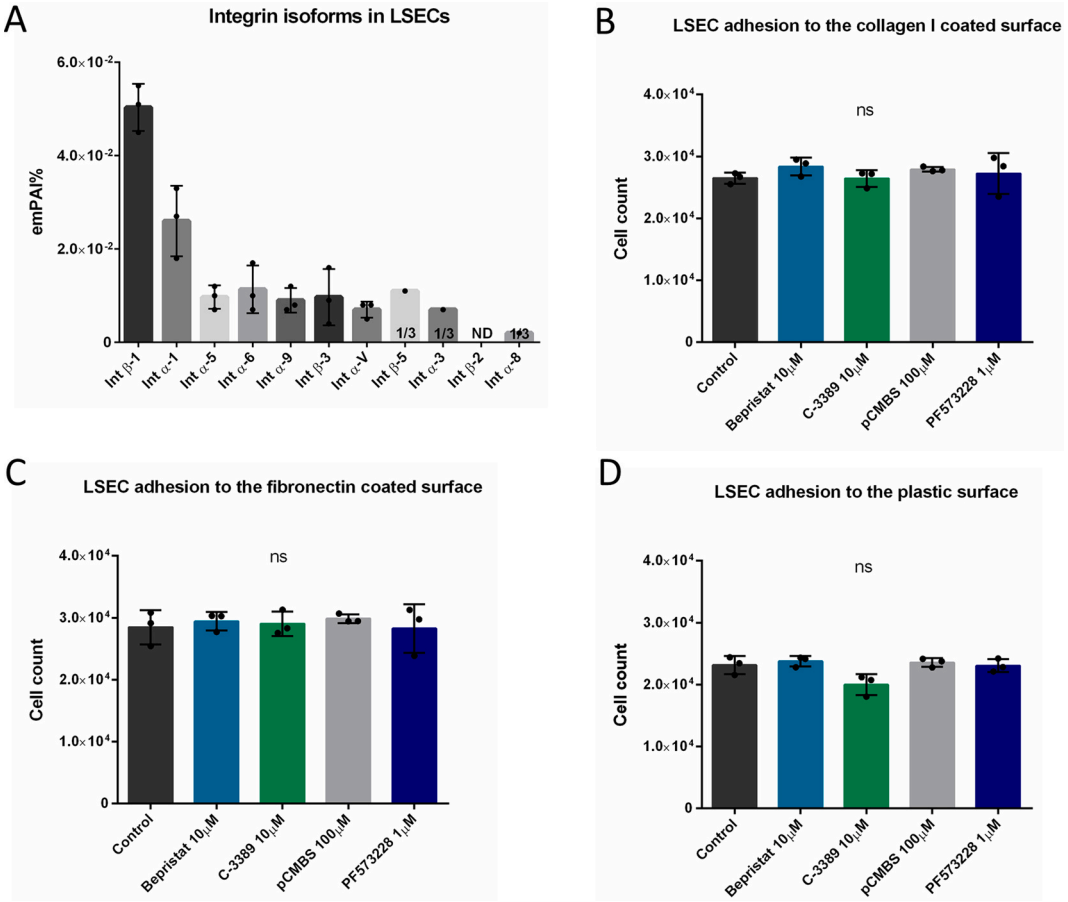

Fig. 4. The effect of PDIA1 inhibition on adhesion of primary mouse LSECs. The repertoire of integrin isoforms detected with proteomic analysis (A) and adhesion efficiency of primary mouse LSECs to the collagen type I (B), fibronectin (C), and uncoated surface (D) after treatment with bepristat, C-3389, pCMBS, and PF573228 (FAK inhibitor). Adhesion experiments were performed in n = 3 biological repeats.
Data are presented as mean values ± SD. ND – not detected; 1/3 – detected in one out of three samples; ns – not statistically significant.

PDIA1 inhibition, regardless of the presence of Y27632, implying that the effects of bepristat were independent of ROCK-mediated myosin phosphorylation (Fig. 7B, C, S4). In contrast to NEM or cytochalasin B, which clearly affected the organisation of the actin filaments in LSECs, there were no visible changes in the actin cytoskeleton in response to C-3389 or bepristat as compared to the untreated cells (Fig. 7D). Of note, the increase in cell stiffness was visible after C-3389, but not after bepristat treatment (Figs. S2A, B, D), which could suggest actin polymerisation and formation of stress fibres induced by C-3389.

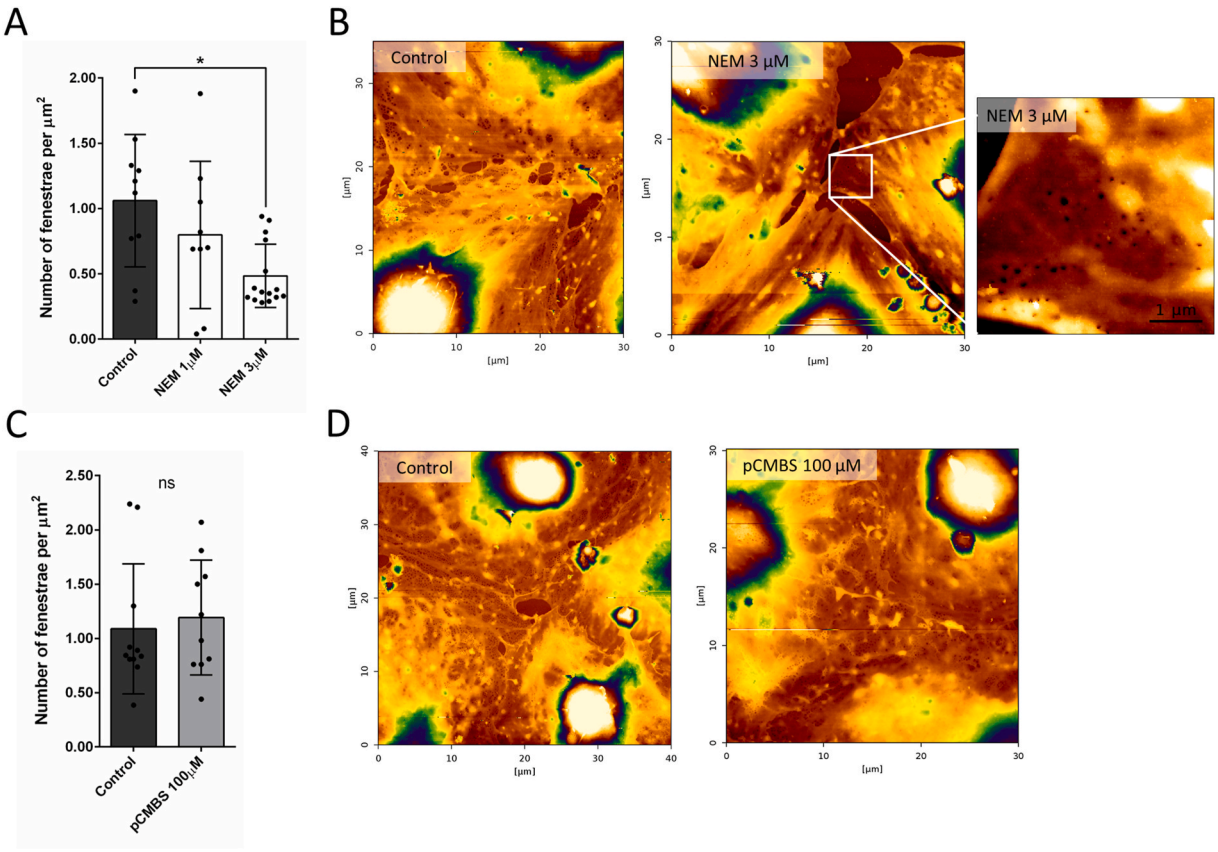

Fig. 5. The effects of modifications of extracellular and intracellular thiol groups on fenestrations in primary mouse LSECs. The mean number of fenestrations and representative images of LSEC topography in response to the cell-permeable NEM (A, B) and cell-impermeable sulfhydryl reagent pCMBS (C, D) measured *in vitro* by AFM.

The graphs show the mean values ± SD for individual AFM images: n = 10–11 for pCMBS and n = 9–15 for NEM, corresponding to two and three biological replicates, respectively. *P ≤ 0.05, significantly different vs control group, ns – not statistically significant.

Importantly, blocking PDIA1 with bepristat did not prevent actin depolymerisation induced by Y27632 (10 µM) or cytochalasin B (21 µM) in LSECs (Fig. 7D). These results are highly consistent with the real-time AFM analysis, which showed that LSEC defenestration induced by bepristat (10 µM) was rapidly reversed upon stimulation with cytochalasin B (21 µM) (Fig. 7E, Movie S4). Despite PDIA1 inhibition, the potential of actin reorganisation in LSECs associated with fenestration formation was fully preserved, which confirms the regulatory role of PDIA1.

Supplementary video can be found at https://doi.org/10.1016/j.redox.2024.103162

4. Discussion

The present study identified the repertoire of PDIs in primary murine LSECs proteome and provided strong evidence for the role of intracellular PDIA1 in regulating fenestration dynamics. It was demonstrated that inhibition of PDIA1 induced significant defenestration of primary LSECs *in vitro*, but did not affect LSEC adhesion, viability, and bioenergetics. PDIA1-dependent LSEC defenestration was not associated with major rearrangement of the actin cytoskeleton, was independent of ROCK-mediated myosin phosphorylation, but was reversible by cytochalasin B – a well-known actin-depolymerising agent and stimulator of LSEC fenestrations. Given the canonical function of PDIs as thiol-disulfide isomerase and oxireductase, it can be concluded that the fenestration dynamics was modulated by PDIA1-dependent intracellular modification of disulfide bonds, although the type of reaction (reduction, oxidation or isomerization) and direct target remain to be identified. Importantly, systemic inhibition of PDIA1 affected intra-parenchymal uptake of contrast agent in mice consistent with LSEC defenestration. Altogether, this work revealed PDIA1 contribution to the physiological regulation of porosity in primary mouse LSECs, which translates into the regulation of hepatic sinusoid perfusion capacity and liver homeostasis *in vivo*.

The key finding of the study was the demonstration of the involvement of PDIA1, but not PDIA3, in maintaining LSEC porosity, even though the expression of the A1 isoform was lower than the A3 isoform in isolated LSECs. In consequence, despite belonging to one enzyme family, both isoforms seemed to be unable to compensate for each other, which proves isoform-specific regulation of fenestrations. Given increasing evidence linking cellular distribution of PDIs and their function [39], the difference in the cellular localisation between PDIA1 and PDIA3 in primary mouse LSECs shown here remains consistent with their distinct activities.

The different roles of PDIA1 and PDIA3 have been previously described in platelet function and have been proposed to result from targeting either intra- or extracellular disulfide exchange mechanisms [4,27]. Similarly, in LSECs, the blockage of intracellular and surface thiols with NEM or pCMBS, respectively, caused distinct effects on fenestrations. pCMBS is a well-known membrane-impermeant inhibitor of disulfide exchange, often used as a reference in PDI studies [5,6,21,40,41], while NEM penetrates cells and alkylates free intracellular thiols making them inaccessible. Many reports investigating PDI-dependent regulation showed the inhibitory effects of pCMBS on platelet aggregation and cancer cell adhesion through irreversible binding to sulfhydryl groups of surface proteins [6,21,41,42]. In primary murine LSECs, modification of extracellular thiols by pCMBS did not affect the number of fenestrations, while treatment with NEM induced a significant

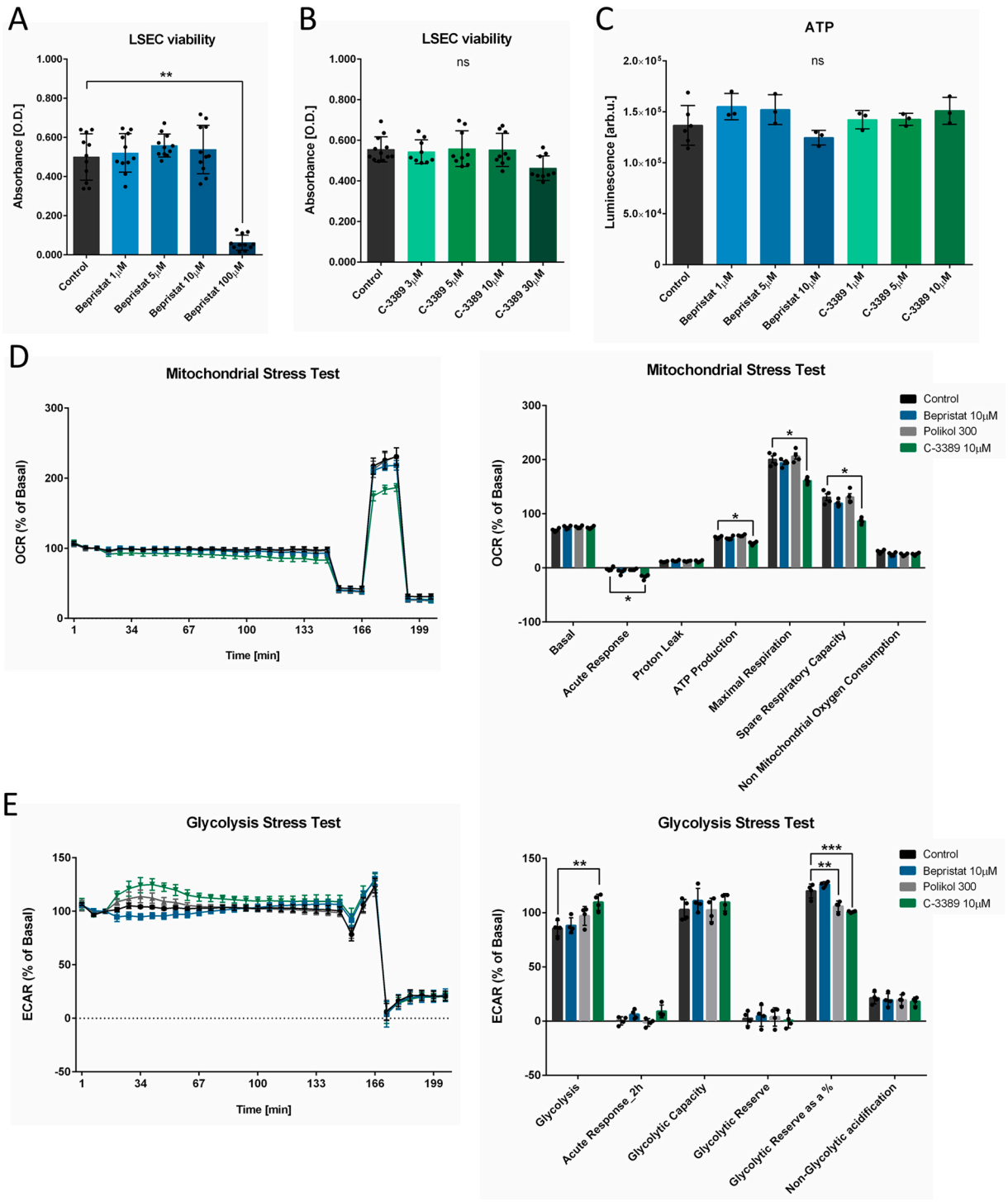

Fig. 6. The effects of PDIA1 inhibition on primary mouse LSEC viability and bioenergetics. LSEC viability (A, B) (n = 3–7) and ATP production (C) measured in the luminescence test (n = 3–6), after 2 h treatment with increasing concentrations of bepristat and C-3389. Mitochondrial (D) and Glycolysis Stress Tests (E) evaluated *in vitro* in primary mouse LSECs in response to bepristat or C-3389 in 10 μM concentrations (n = 4).
Data are presented as mean values ± SD. *P ≤ 0.05, **P ≤ 0.01, ***P ≤ 0.001 significantly different vs control group, ns – not statistically significant.

defenestration. This result indicates that intra- but not extracellular target(s) are involved in the fenestration dynamics, suggesting that intracellular PDIA1-dependent disulfide exchange contributes to the regulation of fenestrations.

The involvement of extracellular disulfide exchange in regulating fenestrations through the modulation of cellular adhesion and integrin outside-in signalling was also excluded. Neither inhibition of PDIA1 nor blockade of the surface sulfhydryls with pCMBS disturbed LSEC adhesion to collagen I, fibronectin, or uncoated surface. These results suggest that in cultured primary mouse LSECs, extracellular disulfide exchange does not regulate cellular adhesion and fenestration dynamics, in opposition to platelets, leukocytes or tumour cells, where extracellular, PDIA1-dependent modification of integrin β1 is involved in the regulation of cell adhesion [3,5,6,21,41,43]. Furthermore, the selective inhibition of FAK, a key signalling molecule responsible for the regulation of integrin function and cellular adhesion, did not affect LSEC

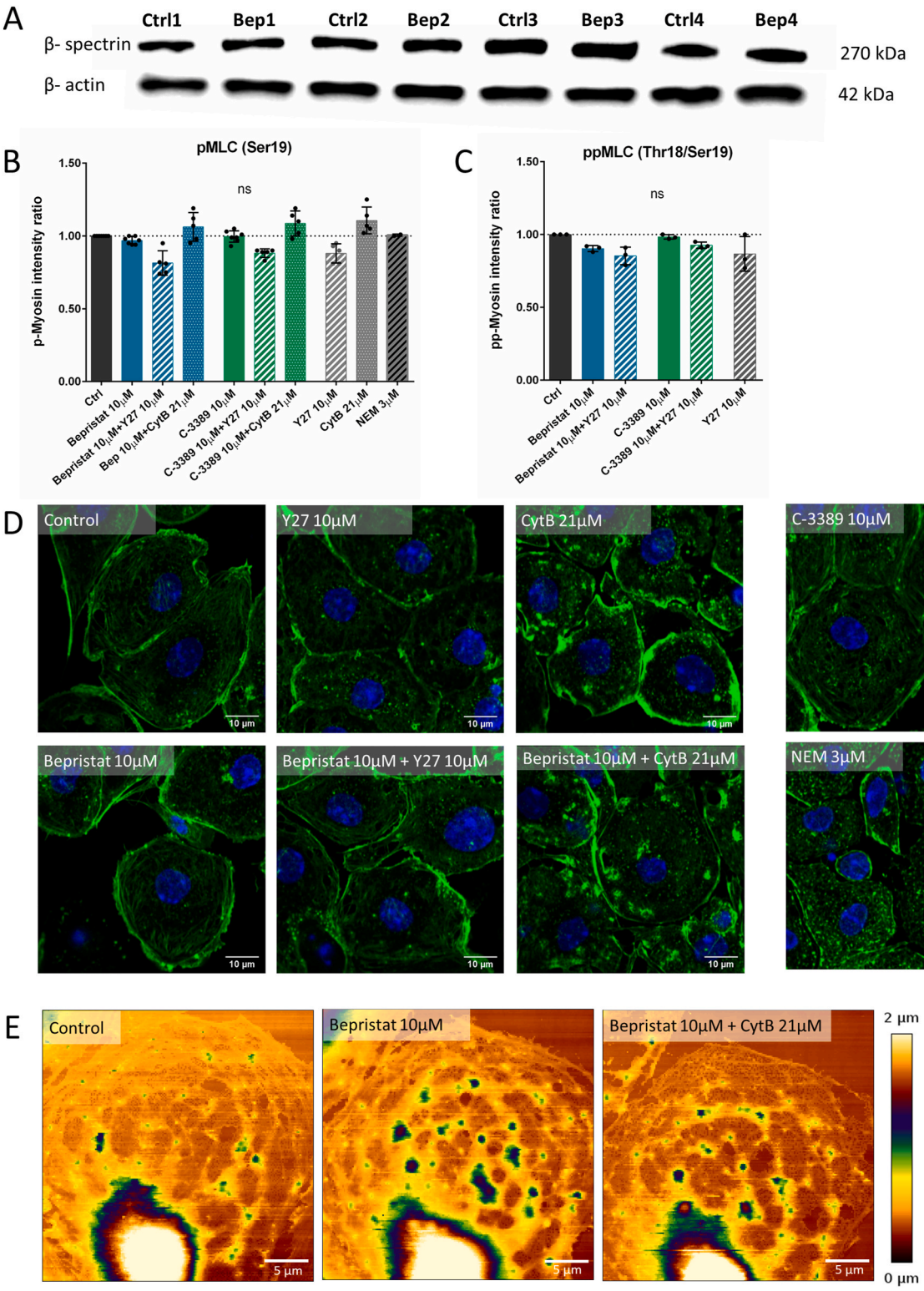

Fig. 7. The Effect of PDIA1 inhibition on LSEC fenestrations reversed by cytochalasin B without major changes in cytoskeleton organisation. Expression of spectrin βII after PDIA1 inhibition (A). Phosphorylation (B) and diphosphorylation (C) of the myosin light chain (MLC) at Ser19 and Thr18/Ser19 induced by cytochalasin B (CytB) and ROCK inhibitor (Y27632), in the presence or absence of PDIA1 inhibitors in primary mouse LSECs. Polymerisation of actin cytoskeleton after treatment with PDIA1 inhibitors, NEM (disulfide blocker), Y27632 and CytB in primary mouse LSECs (D). Reversal of PDIA1-dependent defenestration by 21 μM CytB assessed in living cells using AFM (E).

The scale bars refers to the sample height, where range between 0 and 2.0 μm corresponds to the surface (glass coverslip) and to the highest point of the cell (nucleus), respectively. Fenestrae (white brackets) are visible as dark spots organized in sieve plates at the height corresponding to the surface. ns – not statistically significant.

adhesion. The lack of changes in LSEC adhesion after FAK inhibition may result from impaired mechanotransduction due to LSECs seeding on a stiff surface that does not correspond to the physiological microenvironment [44–46]. On the other hand, during adhesion to collagen I, LSECs were shown to form integrin-independent linear invadosomes [47], which could mask an effect of PDIA1 inhibition on LSEC attachment. Nevertheless, the data provided here suggest that PDIA1-dependent regulation of LSEC fenestrations cannot be attributed to the extracellular PDIA1 function and the regulation of integrin-mediated adhesion or outside-in signalling, although LSECs displayed a wide range of integrins, including the most abundant β1 isoform.

In the present work, a number of other possible mechanisms, such as NOX-derived ROS signalling [8], bioenergetics [48] or substantial structural cytoskeleton rearrangements [19] were also excluded.

Indeed, the interplay between NOX1 and PDIA1 was shown to have a functional role in platelets and VSMC [8,27], and intracellular ROS produced by NADPH oxidases, were reported to act as signalling molecules mediating Rho/ROCK-dependent reorganisation of the acto-myosin cytoskeleton [49,50]. Due to the limited availability of isoform-specific pharmacological tools for NOX inhibition, the study was performed using relatively selective ML171. Despite its strong preference towards NOX1, this compound can still show activity towards other isoforms, as well as glucose oxidase and xanthine oxidase [51]. In contrast to PDIA1 inhibition, even unspecific blocking of multiple NOX isoforms did not affect LSEC porosity, although it effectively inhibited ROS formation. Distinct effects of bepristat and ML171 suggest that the function of PDIA1 in maintaining fenestrations in LSECs was not related to NOX-mediated ROS signalling and was different from mechanisms described for PDI-dependent and ROS-dependent regulation in platelets or VSMC [8,27].

It also seems unlikely that the PDIA1 target responsible for the regulation of fenestrations in LSECs is located in the mitochondria. Although PDIA1 was found to protect endothelial cells from excess ROS and its negative effect through the control of mitochondrial fusion and fission [52], PDIA1 inhibitors inducing defenestration were not associated with significant changes in LSEC bioenergetics. This result indicates that the regulation of fenestrations by PDIA1 is independent of mitochondrial respiration.

On the other hand, it can be speculated that PDIA1-dependent regulation of fenestration dynamics in LSECs could be linked to the cytoskeleton remodeling, however not through the direct modifications of the major structural proteins of the cytoskeleton, but rather by subtle redox-dependent regulation of ancillary actin protein(s) or upstream signalling. In fact, the effect of PDIA1 inhibition on fenestration dynamics in LSECs was not associated with clear-cut changes in actin polymerisation, myosin phosphorylation, or spectrin disruption. In contrast, modification of sulfhydryls by NEM or with diamide [19] resulted in actin and spectrin destabilisation, respectively. Different patterns of LSEC responses may suggest that the potential mechanism of PDIA1 action is distinct as compared with previously reported mechanisms demonstrating cytoskeleton rearrangement via sulfhydryl modifications [5,8,53].

In this context, it was an important finding of this work to demonstrate that stimulation with cytochalasin B reversed LSEC defenestration after bepristat treatment. Cytochalasins – actin-depolymerising gold standards – induced fenestrations in dedifferentiated LSECs after six days of culturing [12,54], but did not increase LSEC porosity after irreversible cytoskeletal changes, such as microtubule disruption induced by paclitaxel [55] or inhibition of myosin light chain (MLC) phosphorylation by ML-7 [56]. Moreover, treatment of primary LSECs with either colchicine or taxol, both tubulin-disrupting agents, did not affect LSEC porosity despite significant loss of microtubules [55]. The intact architecture of the cytoskeleton is, therefore, critical to preserving the ability of the LSEC to form fenestrations in response to cytochalasin. Thus, the lack of changes in the cytoskeleton structural proteins after PDIA1 inhibition together with the preserved ability to form new pores in response to cytochalasin B points to a regulatory role of PDIA1 and targeting of a distinct redox-regulated protein, important for maintaining fenestration dynamics in LSECs.

In fact, many redox-sensitive proteins have been identified in the cytoskeleton regulatory network, although the role of the oxidation of these proteins on cellular functions remains largely to be determined [57]. Several targets including regulatory and anchor proteins of the cytoskeleton could therefore interact with the multidomain thioredoxin structure of PDIA1. Susceptibility to redox status has, for example, been shown for cofilin, an actin-binding protein disassembling actin filaments. Oxidative modifications of cysteine residues of cofilin resulted in its inactivation and impaired cell motility in mesenchymal cells, cardiomyocytes, and T-cells [58–60], which may also be relevant for LSEC porosity. Moreover, extensive studies on red blood cell (RBC) mechanoproperties and deformability revealed that ankyrin might represent another molecular target regulated by cysteine redox switches in addition to the direct oxidation of spectrin [61,62]. Ankyrin binds spectrin to the cell membrane, facilitating rapid changes of RBC morphology during squeezing through the capillaries [62,63], which, to some extent, might resemble the rapid dynamics of fenestrations in LSECs. Apart from cofilin, and ankyrin, there are other possible targets for PDIA1 in the actin-regulatory network or in the signalling pathways mediating cytoskeleton rearrangement such as Cdc 42, Src, or PKC [57], however, their involvement in LSEC porosity is still not fully understood. Of note, the activities of PDI family members have been shown to be calcium-dependent [64]. Therefore, a possible target of PDIA1 action on LSEC fenestrations might also be related to calmodulin and calcium homeostasis. Previously, an inhibitor of calmodulin-dependent protein kinase II (KN93) was shown to decrease LSEC porosity with no alterations in actin or myosin structures, as the calcium-independent myosin phosphorylation pathway was still active [56]. Moreover, defenestration was reversed by cytochalasin B, providing a phenotypically similar response to that reported here for PDIA1 inhibition. Taken together, current knowledge about the mechanisms regulating fenestrations is still very limited [49], and this work has identified a new player involved – PDIA1, which had not previously been taken into consideration in this complex machinery. However, the molecular mechanism of PDIA1-dependent regulation of fenestration dynamics in LSECs remains to be determined.

Currently, targeting PDIs sets a new direction in therapeutical approaches to cancer and thrombosis. In particular, PDI inhibitors are considered promising pharmacological tools as they have been shown to effectively suppress ovarian tumour growth or reduce colorectal cancer malignancy [65,66]. Unfortunately, most available compounds are non-selective or cell-penetrating, modifying intracellular PDI function and thus affecting other intracellular mechanisms. The key finding of this study, demonstrating PDIA1-dependent LSEC defenestration, is a striking example of the physiological consequences of intracellular PDIA1 inhibition. On the other hand, given that the inhibition of extracellular PDIs is also effective in limiting cancer cell and leukocyte adhesion, as well as platelet adhesion and aggregation [3,21,27], the pharmacology of platelets or tumour metastasis should be targeted to extracellular rather than intracellular PDIs to avoid disrupting fenestration dynamics.

It is well established that maintaining the correct fenestration dynamics is crucial for liver function and the defenestration of LSECs is an early hallmark of impaired hepatic microcirculation [37,38]. Hepatic perfusion capacity consists mainly of the sinusoid lumen and space of Disse separated by the fenestrated endothelial layer [9]. This unique morphology determines the volume of perfusion, blood flow velocity and blood-liver homeostasis [10,11]. Efficient fenestrations are responsible for the filtration properties of LSECs ensuring bidirectional transport of fluids and substances, especially lipoproteins, between liver sinusoids and hepatocytes. Lack of fenestrations may result in profound hyperlipoproteinemia and liver steatosis as demonstrated in

plasmalemma vesicle-associated protein (PLVAP) deficient mice [18]. DCE-MRI, commonly used in the clinic to assess liver status, was used here to demonstrate alterations in the sinusoidal perfusion after PDIA1 inhibition *in vivo*. In this method, the intensity of the registered signal depends on the perfusion, vascular permeability, and the size of the extravascular and extracellular space, which are partially maintained by LSEC porosity [18,34,36]. The systemic inhibition of PDIA1 was accompanied by significant impairment in contrast agent uptake in the liver parenchyma consistent with PDIA1-dependent LSEC defenestration *in vitro*. The observed changes were rather not related to cardiac dysfunction or hepatocyte damage, as was the case in a murine model of chronic heart failure [67] or concavalin A-induced hepatocyte damage [34]. The most likely cause was direct inhibition of PDIA1 resulting in LSEC defenestration, thus limiting the sinusoidal perfusion volume. The comparable effects of the poloxamer 407 pre-treatment on DCE-MRI readout, seem to support this hypothesis. It can therefore be concluded that pharmacological inhibition of intracellular PDIA1 *in vivo* leads to compromised sinusoidal perfusion and disturbances of hepatic sinusoidal homeostasis.

This study has several limitations that need to be highlighted. Although an attempt was made to gain insight into the molecular mechanisms of PDIA1-dependent defenestration, and NOX-mediated ROS signalling, bioenergetics, or cytoskeleton rearrangement were excluded, in the latter aspect this work focused exclusively on the major structural proteins of the cytoskeleton, which were previously linked to the fenestration dynamics and their structure [49]. However, many anchor and regulatory proteins play a role in cytoskeleton reorganisation, and could constitute a potential target for PDIA1 action as discussed above. Moreover, the current study did not determine what type of PDI-dependent reaction maintains LSEC fenestrations (reduction, oxidation or isomerization) and whether one or multiple cysteine residues of a target protein were involved. Therefore, further studies with different experimental approaches [5] are needed to reveal details of the mechanism by which PDIA1 inhibition induces LSEC defenestration. Finally, although two inhibitors of PDIA1, with different chemical structure and different mechanisms of action [22,68], showed concordant results regarding the involvement of PDIA1 in the regulation of LSEC fenestrations, additional studies using gene silencing approach or tissue-selective mouse knockout models could further support this conclusion.

Despite these limitations, the presented results extend the knowledge of the mechanisms responsible for maintaining LSEC porosity, showing that intracellular PDIA1 regulates fenestration dynamics and maintains homeostasis of hepatic sinusoids. The PDIA1-mediated mechanism of action appears to be independent of integrins and ecto-sulfhydryls, NOX, or mitochondrial ROS signalling, and did not involve robust alterations in cytoskeleton organisation. Most likely, the function of PDIA1 in maintaining LSEC porosity involves subtle regulation of the redox-sensitive cytoskeletal microarchitecture. Importantly, the presented results have not only pathophysiological significance and foster further studies on redox-dependent regulation of fenestrations, but also have clinical relevance due to the growing interest in novel therapeutic strategies targeting PDIA1. Given the fundamental role of intracellular PDIA1 in maintaining fenestrations in LSECs, targeting extracellular PDIs appears to be a safer therapeutic approach to avoid defenestration after PDIA1 inhibition in the liver.

Availability of data and materials

The proteomic dataset have been deposited in the RODBUK Cracow Open Research Data Repository with the identifier https://doi.org/10.26106/1s6v-t189. The remaining data, analytic methods, and study materials will be available from the corresponding authors on reasonable request.

CRediT authorship contribution statement

Izabela Czyzynska-Cichon: Writing – original draft, Visualization, Methodology, Investigation, Formal analysis, Conceptualization. **Magdalena Giergiel:** Writing – review & editing, Software, Formal analysis. **Grzegorz Kwiatkowski:** Writing – review & editing, Methodology, Investigation, Formal analysis. **Anna Kurpinska:** Writing – review & editing, Investigation, Formal analysis. **Kamila Wojnar-Lason:** Writing – review & editing, Investigation, Formal analysis. **Patrycja Kaczara:** Writing – review & editing, Investigation, Formal analysis. **Marek Szymonski:** Writing – review & editing, Resources. **Malgorzata Lekka:** Writing – review & editing, Resources. **Ivars Kalvins:** Writing – review & editing, Resources. **Bartlomiej Zapotoczny:** Writing – review & editing, Project administration, Investigation, Funding acquisition, Formal analysis. **Stefan Chlopicki:** Writing – review & editing, Supervision, Resources, Conceptualization.

Declaration of competing interest

The authors declare that they have no known competing financial interests or personal relationships that could have appeared to influence the work reported in this paper.

Data availability

The link to the proteomic dataset repository is provided in the manuscript. The remaining data will be available on request.

Acknowledgments

This work was supported by the National Science Centre (Poland) SONATA 15 program (grant no. 2019/35/D/NZ3/01804).

The confocal imaging was performed in the Laboratory of *in vivo* and *in vitro* Imaging of Maj Institute of Pharmacology, Polish Academy of Sciences.

The equipment used for this work was sponsored in part by the Centre for Preclinical Research and Technology (CePT), a project cosponsored by the European Regional Development Fund and Innovative Economy, The National Cohesion Strategy of Poland.

The authors thank Agata Malinowska from Mass Spectrometry Laboratory, Institute of Biochemistry and Biophysics, Polish Academy of Sciences, Warsaw, Poland for LC-MS data acquisition.

Appendix A. Supplementary data

Supplementary data to this article can be found online at https://doi.org/10.1016/j.redox.2024.103162.

References

[1] S. Parakh, J.D. Atkin, Novel roles for protein disulphide isomerase in disease states: a double edged sword? Front. Cell Dev. Biol. 3 (2015) 30.

[2] R.F. Goldberger, C.J. Epstein, C.B. Anfinsen, Acceleration of reactivation of reduced bovine pancreatic ribonuclease by a microsomal system from rat liver, J. Biol. Chem. 238 (1963).

[3] T.A. Bennett, B.S. Edwards, L.A. Sklar, S. Rogelj, Sulfhydryl regulation of L-selectin shedding: phenylarsine oxide promotes activation-independent L-selectin shedding from leukocytes, J. Immunol. 164 (8) (2000).

[4] L. Wang, Y. Wu, J. Zhou, S.S. Ahmad, B. Mutus, N. Garbi, et al., Platelet-derived ERp57 mediates platelet incorporation into a growing thrombus by regulation of the αIIbβ3 integrin, Blood 122 (22) (2013).

[5] K. Sobierajska, S. Skurzynski, M. Stasiak, J. Kryczka, C.S. Cierniewski, M. Swiatkowska, Protein disulfide isomerase directly interacts with β-actin Cys 374 and regulates cytoskeleton reorganization, J. Biol. Chem. 289 (9) (2014).

[6] M. Popielarski, H. Ponamarczuk, M. Stasiak, L. Michalec, R. Bednarek, M. Studzian, et al., The role of Protein Disulfide Isomerase and thiol bonds modifications in activation of integrin subunit alpha 11, Biochem. Biophys. Res. Commun. 495 (2) (2018).

[7] H. Ponamarczuk, M. Popielarski, M. Stasiak, R. Bednarek, M. Studzian, L. Pulaski, et al., Contribution of activated beta 3 integrin in the PDI release from endothelial cells, Frontiers in Bioscience - Landmark 23 (9) (2018).

[8] L.A. Pescatore, D. Bonatto, F.L. Forti, A. Sadok, H. Kovacic, F.R.M. Laurindo, Protein disulfide isomerase is required for platelet-derived growth factor-induced vascular smooth muscle cell migration, Nox1 NADPH oxidase expression, and RhoGTPase activation, J. Biol. Chem. 287 (35) (2012).

[9] A. Blouin, R.P. Bolender, E.R. Weibel, Distribution of organelles and membranes between hepatocytes and nonhepatocytes in the rat liver parenchyma, J. Cell Biol. 72 (1977) 441–455.

[10] T. Wang, S. Lü, Y. Hao, Z. Su, M. Long, Y. Cui, Influence of microflow on hepatic sinusoid blood flow and red blood cell deformation, Biophys. J. 120 (21) (2021 Nov 2) 4859–4873.

[11] K.K. Sørensen, P. McCourt, T. Berg, C. Crossley, D. Le Couteur, K. Wake, et al., The scavenger endothelial cell: a new player in homeostasis and immunity, Physiology Am J Physiol Regul Integr Comp Physiol 303 (2012) 1217–1230.

[12] N.J. Hunt, G.P. Lockwood, A. Warren, H. Mao, P.A.G. McCourt, D.G. le Couteur, et al., Manipulating fenestrations in young and old liver sinusoidal endothelial cells, Am. J. Physiol. Gastrointest. Liver Physiol. 316 (1) (2019).

[13] M. Miyao, H. Kotani, T. Ishida, C. Kawai, S. Manabe, H. Abiru, et al., Pivotal role of liver sinusoidal endothelial cells in NAFLD/NASH progression, Lab. Invest. 95 (10) (2015).

[14] M. Bravo, I. Raurell, D. Hide, A. Fernández-Iglesias, M. Gil, A. Barberá, et al., Restoration of liver sinusoidal cell phenotypes by statins improves portal hypertension and histology in rats with NASH, Sci. Rep. 9 (1) (2019).

[15] B. Xu, U. Broome, M. Uzunel, S. Nava, X. Ge, M. Kumagai-Braesch, et al., Capillarization of hepatic sinusoid by liver endothelial cell-reactive autoantibodies in patients with cirrhosis and chronic hepatitis, Am. J. Pathol. 163 (4) (2003).

[16] M. Xu, H.H. Xu, Y. Lin, X. Sun, L.J. Wang, Z.P. Fang, et al., LECT2, a ligand for Tie 1, plays a crucial role in liver fibrogenesis, Cell 178 (6) (2019).

[17] A. Baiocchini, F del Nonno, C. Taibi, U. Visco-Comandini, G. D'Offizi, M. Piacentini, et al., Liver sinusoidal endothelial cells (LSECs) modifications in patients with chronic hepatitis C, Sci. Rep. 9 (1) (2019).

[18] L. Herrnberger, R. Hennig, W. Kremer, C. Hellerbrand, A. Goepferich, H. R. Kalbitzer, et al., Formation of fenestrae in murine liver sinusoids depends on plasmalemma vesicle-associated protein and is required for lipoprotein passage, PLoS One 9 (12) (2014 Dec 26).

[19] B. Zapotoczny, F. Braet, E. Kus, K. Ginda-Mäkelä, B. Klejevskaja, R. Campagna, et al., Actin-spectrin scaffold supports open fenestrae in liver sinusoidal endothelial cells, Traffic 20 (12) (2019).

[20] Y. Wu, D.W. Essex, Vascular thiol isomerases in thrombosis: the yin and yang, J. Thromb. Haemostasis 18 (11) (2020).

[21] M. Stojak, M. Milczarek, A. Kurpinska, J. Suraj-Prazmowska, P. Kaczara, K. Wojnar-Lason, et al., Protein disulphide isomerase a1 is involved in the regulation of breast cancer cell adhesion and transmigration via lung microvascular endothelial cells, Cancers 12 (10) (2020).

[22] D. Zelencova-Gopejenko, V. Andrianov, I. Domracheva, I. Kanepe-Lapsa, M. Milczarek, M. Stojak, et al., Aromatic sulphonamides of aziridine-2-carboxylic acid derivatives as novel PDIA1 and PDIA3 inhibitors, J. Enzym. Inhib. Med. Chem. 38 (1) (2023).

[23] B. Smedsrod, H. Pertoft, Preparation of pure hepatocytes and reticuloendothelial cells in high yield from a single rat liver by means of Percoll centrifugation and selective adherence, J. Leukoc. Biol. 38 (2) (1985).

[24] E. Kus, P. Kaczara, I. Czyzynska-Cichon, K. Szafranska, B. Zapotoczny, A. Kij, et al., LSEC fenestrae are preserved despite pro-inflammatory phenotype of liver sinusoidal endothelial cells in mice on high fat diet, Front. Physiol. 10 (FEB) (2019).

[25] B. Zapotoczny, F. Braet, E. Wisse, M. Lekka, M. Szymonski, Biophysical nanocharacterization of liver sinusoidal endothelial cells through atomic force microscopy, in: Biophysical Reviews, vol. 12, 2020.

[26] B. Sitek, D.M. Waldera-Lupa, G. Poschmann, H.E. Meyer, K. Stühler, Application of label-free proteomics for differential analysis of lung carcinoma cell line A549, Methods Mol. Biol. 893 (2012).

[27] K. Przyborowski, A. Kurpinska, D. Wojkowska, P. Kaczara, J. Suraj-Prazmowska, K. Karolczak, et al., Protein disulfide isomerase-A1 regulates intraplatelet reactive oxygen species–thromboxane A2-dependent pathway in human platelets, J. Thromb. Haemostasis 20 (1) (2022).

[28] A. Malinowska, M. Kistowski, M. Bakun, T. Rubel, M. Tkaczyk, J. Mierzejewska, et al., Diffprot - software for non-parametric statistical analysis of differential proteomics data, J. Proteonomics 75 (13) (2012).

[29] J.E. Elias, W. Haas, B.K. Faherty, S.P. Gygi, Comparative evaluation of mass spectrometry platforms used in large-scale proteomics investigations, Nat. Methods 2 (9) (2005).

[30] J. Roy, K.L. Wycislo, H. Pondenis, T.M. Fan, A. Das, Comparative proteomic investigation of metastatic and non-metastatic osteosarcoma cells of human and canine origin, PLoS One 12 (9) (2017).

[31] Y. Ishihama, Y. Oda, T. Tabata, T. Sato, T. Nagasu, J. Rappsilber, et al., Exponentially modified protein abundance index (emPAI) for estimation of absolute protein amount in proteomics by the number of sequenced peptides per protein, Mol. Cell. Proteomics 4 (9) (2005).

[32] B. Zapotoczny, K. Szafranska, E. Kus, S. Chlopicki, M. Szymonski, Quantification of fenestrations in liver sinusoidal endothelial cells by atomic force microscopy, Micron 101 (2017).

[33] M. Giergiel, B. Zapotoczny, I. Czyzynska-Cichon, J. Konior, M. Szymonski, AFM image analysis of porous structures by means of neural networks, Biomed. Signal Process Control 71 (2022).

[34] K. Byk, K. Jasinski, Z. Bartel, A. Jasztal, B. Sitek, B. Tomanek, et al., MRI-based assessment of liver perfusion and hepatocyte injury in the murine model of acute hepatitis, Magnetic Resonance Materials in Physics, Biology and Medicine 29 (6) (2016 Dec 1) 789–798.

[35] A. Kij, A. Bar, I. Czyzynska-Cichon, K. Przyborowski, B. Proniewski, L. Mateuszuk, et al., Vascular protein disulfide isomerase A1 mediates endothelial dysfunction induced by angiotensin II in mice, Acta Physiol. 23 (2024 Feb) e14116.

[36] V.C. Cogger, S.N. Hilmer, D. Sullivan, M. Muller, R. Fraser, D.G. Le Couteur, Hyperlipidemia and surfactants: the liver sieve is a link, Atherosclerosis 189 (2) (2006 Dec) 273–281.

[37] S.N. Hilmer, V.C. Cogger, R. Fraser, A.J. McLean, D. Sullivan, D.G. Le Couteur, Age-related changes in the hepatic sinusoidal endothelium impede lipoprotein transfer in the rat, Hepatology 42 (6) (2005 Dec) 1349–1354.

[38] S.J. Mitchell, A. Huizer-Pajkos, V.C. Cogger, A.J. McLachlan, D.G. Le Couteur, B. Jones, et al., The influence of old age and poloxamer-407 on the hepatic disposition of diazepam in the isolated perfused rat liver, Pharmacology 90 (5–6) (2012).

[39] C. Turano, S. Coppari, F. Altieri, A. Ferraro, Proteins of the PDI family: unpredicted non-ER locations and functions, J. Cell. Physiol. 193 (2) (2002).

[40] K. Jurk, J. Lahav, H. van Aken, M.F. Brodde, J.R. Nofer, B.E. Kehrel, Extracellular protein disulfide isomerase regulates feedback activation of platelet thrombin generation via modulation of coagulation factor binding, J. Thromb. Haemostasis 9 (11) (2011).

[41] J. Lahav, K. Jurk, O. Hess, M.J. Barnes, R.W. Farndale, J. Luboshitz, et al., Sustained integrin ligation involves extracellular free sulfhydryls and enzymatically catalyzed disulfide exchange, Blood 100 (7) (2002).

[42] N. Manickam, X. Sun, K.W. Hakala, S.T. Weintraub, D.W. Essex, Thiols in the αIIbβ3 integrin are necessary for platelet aggregation, Br. J. Haematol. 142 (3) (2008).

[43] I.H. Chen, F.R. Chang, Y.C. Wu, P.H. Kung, C.C. Wu, 3,4-Methylenedioxy-β-nitrostyrene inhibits adhesion and migration of human triple-negative breast cancer cells by suppressing β1 integrin function and surface protein disulfide isomerase, Biochimie 110 (2015) 81–92.

[44] A. Juin, E. Planus, F. Guillemot, P. Horakova, C. Albiges-Rizo, E. Génot, et al., Extracellular matrix rigidity controls podosome induction in microvascular endothelial cells, Biol. Cell. 105 (1) (2013).

[45] A.J. Ford, G. Jain, P. Rajagopalan, Designing a fibrotic microenvironment to investigate changes in human liver sinusoidal endothelial cell function, Acta Biomater. 24 (2015).

[46] P. Li, J. Zhou, W. Li, H. Wu, J. Hu, Q. Ding, et al., Characterizing liver sinusoidal endothelial cell fenestrae on soft substrates upon AFM imaging and deep learning, Biochim. Biophys. Acta Gen. Subj. 1864 (12) (2020).

[47] A. Juin, C. Billotteta, V. Moreau, O. Destaing, C. Albiges-Rizo, J. Rosenbaum, et al., Physiological type I collagen organization induces the formation of a novel class of linear invadosomes, Mol. Biol. Cell 23 (2) (2012 Jan 15) 297–309.

[48] F. Braet, M. Muller, K. Vekemans, E. Wisse, D.G. le Couteur, Antimycin A-induced defenestration in rat hepatic sinusoidal endothelial cells, Hepatology 38 (2) (2003).

[49] K. Szafranska, L.D. Kruse, C.F. Holte, P. McCourt, B. Zapotoczny, The wHole story about fenestrations in LSEC, Front. Physiol. 12 (2021).

[50] E.N. Popova, O.Y. Pletjushkina, V.B. Dugina, L.v. Domnina, O.Y. Ivanova, D. S. Izyumov, et al., Scavenging of reactive oxygen species in mitochondria induces myofibroblast differentiation, Antioxidants Redox Signal. 13 (9) (2010).

[51] F.L.M. Szekeres, E. Walum, P. Wikström, A. Arner, A small molecule inhibitor of Nox 2 and Nox 4 improves contractile function after ischemia–reperfusion in the mouse heart, Sci. Rep. 11 (1) (2021 Dec 1).

[52] Y.M. Kim, S.W. Youn, V. Sudhahar, A. Das, R. Chandhri, H. Cuervo Grajal, et al., Redox regulation of mitochondrial fission protein drp 1 by protein disulfide isomerase limits endothelial senescence, Cell Rep. 23 (12) (2018).

[53] L.Y. Tanaka, H.A. Araújo, G.K. Hironaka, T.L.S. Araujo, C.K. Takimura, A. I. Rodriguez, et al., Peri/epicellular protein disulfide isomerase sustains vascular lumen caliber through an anticonstrictive remodeling effect, Hypertension 67 (3) (2016).

[54] J. di Martino, P. Mascalchi, P. Legros, S. Lacomme, E. Gontier, P. Bioulac-Sage, et al., Actin depolymerization in dedifferentiated liver sinusoidal endothelial cells promotes fenestrae Re-formation, Hepatol Commun 3 (2) (2019).

[55] F. Braet, R. De Zanger, W. Kalle, A. Raap, H. Tanke, E. Wisse, Comparative scanning, transmission and atomic force microscopy of the microtubular cytoskeleton in fenestrated liver endothelial cells, Scanning Microsc. 10 (Suppl. 1996).

[56] B. Zapotoczny, K. Szafranska, M. Lekka, B.S. Ahluwalia, P. McCourt, Tuning of liver sieve: the interplay between actin and myosin regulatory light chain regulates fenestration size and number in murine liver sinusoidal endothelial cells, Int. J. Mol. Sci. 23 (17) (2022 Sep 1).

[57] Q. Xu, L.P. Huff, M. Fujii, K.K. Griendling, Redox regulation of the actin cytoskeleton and its role in the vascular system, Free Radic. Biol. Med. 109 (2017) 84–107. Elsevier Inc.

[58] J.M. Cameron, M. Gabrielsen, Y.H. Chim, J. Munro, E.J. McGhee, D. Sumpton, et al., Polarized cell motility induces hydrogen peroxide to inhibit cofilin via cysteine oxidation, Curr. Biol. 25 (11) (2015).

[59] M. Pignataro, G. di Rocco, L. Lancellotti, F. Bernini, K. Subramanian, E. Castellini, et al., Phosphorylated cofilin-2 is more prone to oxidative modifications on Cys 39 and favors amyloid fibril formation, Redox Biol. 37 (2020).

[60] Y. Samstag, I. John, G.H. Wabnitz, Cofilin: a redox sensitive mediator of actin dynamics during T-cell activation and migration, Immunol. Rev. 256 (1) (2013).

[61] F. Barbarino, L. Wäschenbach, V. Cavalho-Lemos, M. Dillenberger, K. Becker, H. Gohlke, et al., Targeting spectrin redox switches to regulate the mechanoproperties of red blood cells, Biol. Chem. 402 (2021).

[62] W. Sae-Lee, C.L. McCafferty, E.J. Verbeke, P.C. Havugimana, O. Papoulas, C. D. McWhite, et al., The protein organization of a red blood cell, Cell Rep. 40 (3) (2022 Jul 19).
[63] T. Ruskovska, S.J. Bennett, C.R. Brown, S. Dimitrov, N. Kamcev, H.R. Griffiths, Ankyrin is the major oxidised protein in erythrocyte membranes from end-stage renal disease patients on chronic haemodialysis and oxidation is decreased by dialysis and vitamin C supplementation, Free Radic. Res. 49 (2) (2015).
[64] M. Michalak, J.M.R. Parker, M. Opas, Ca2+ signaling and calcium binding chaperones of the endoplasmic reticulum, Cell Calcium 32 (2002).
[65] S. Xu, A.N. Butkevich, R. Yamada, Y. Zhou, B. Debnath, R. Duncan, et al., Discovery of an orally active small-molecule irreversible inhibitor of protein disulfide isomerase for ovarian cancer treatment, Proc. Natl. Acad. Sci. U.S.A. 109 (40) (2012).
[66] Y.S. Ma, S. Feng, L. Lin, H. Zhang, G.H. Wei, Y.S. Liu, et al., Protein disulfide isomerase inhibits endoplasmic reticulum stress response and apoptosis via its oxidoreductase activity in colorectal cancer, Cell. Signal. 86 (2021).
[67] K. Wojnar-Lason, U. Tyrankiewicz, A. Kij, A. Kurpinska, P. Kaczara, G. Kwiatkowski, et al., Chronic heart failure induces early defenestration of liver sinusoidal endothelial cells (LSECs) in mice, Acta Physiol. (2024 Feb 23) e14114.
[68] R.H. Bekendam, P.K. Bendapudi, L. Lin, P.P. Nag, J. Pu, D.R. Kennedy, et al., A substrate-driven allosteric switch that enhances PDI catalytic activity, Nat. Commun. (2016 Aug 30) 7.